Received: 15 February 2022 | Revised: 07 April 2022 | Accepted: 26 March 2022
DOI: 10.22034/ecc.2022.329803.1327
Eurasian Chemical Communications
SAMI

FULL PAPER

Investigation of the π-bridge role for imidazole derivative dyes in dye sensitized solar cell: theoretical study

Saifaldeen Fahim Abdulhussein[a] |Saifaldeen Muwafag Abdalhadi[b,*] |Haitham Dalol Hanoon[a]

[a]*Department of Chemistry, College of Science, University of Kerbala, Kerbala, Iraq*

[b]*Department of Remote Sensing, College of Remote Sensing and Geophysics, Al-Karkh University of Science, Baghdad, Iraq*

A series of metal-free imidazole derivative dyes (C2, C3, C4, and C5) are virtually designed based on the original synthesized dye (*E*)-3-(5-(4,5-bis(4-(diphenylamino)phenyl)-1-ethyl-1*H*-imidazol-2-yl)thiophen-2-yl)-2-cyanoacrylic acid (C1). All these dyes are designed by varying the π-bridge parts for dye-synthesized solar cells. The photovoltaic and optoelectronic properties have been investigated theoretically by using density functional theory (DFT) and time-dependent density functional theory (TD-DFT) methods. Many parameters have been investigated and evaluated to influence the modulation of the π-bridge groups. The optimization geometries, electronic structures, electronic absorption spectra, highest occupied molecular orbital (HOMO), lowest unoccupied molecular orbital (LUMO), energy gap, and oscillator strength of all these dyes were characterized and investigated theoretically. From the results, the C2 dye (with two thiophene molecules as a spacer) was shown to have the lowest energy gap (1.91 eV) and the lowest LUMO, which indicates that the dye has the best electron injection to the TiO_2 surface than other dyes.

***Corresponding Author:**
Saifaldeen Muwafag Abdalhadi
Email: dr.saifaldeen@kus.edu.iq
Tel.: 009647702777191

KEYWORDS

DSSCs; imidazole; π-Bridge; energy gapand density functional theory.

Introduction

The third-generation solar cell is one of the most important technologies in the last two decades due to its high efficiency and environmental friendliness [1]. Nowadays most commercial solar cell panels are currently made from silicon or inorganic semiconductor, and these panels are expensive as silicon and other inorganic semiconductors was being rised in cost dramatically [2]. Therefore, many types of solar cells appear to be promising for clean energy such as organic, quantum dot, and perovskite solar cells due to their low-cost manufacturing, possible flexibility, and low toxicity [3,4]. Dye synthesized solar cells (DSSCs) is one of the most popular methods for third-generation solar cells to generate clean energy, owing to the advantages of this solar cell, such as chemical versatility of the dye, colorful appearances, and a broad synthetic method which leads to design different molecular structures as an active layer in DSSCs [5-7].

The dye design is critical in DSSCs' ability to convert sunlight to electric power. Dyes used for DSSCs should have special photophysical and electrochemical properties such as luminescence, ultraviolet-visible

absorption region, high HOMO, low LUMO, and hydrophobic character [8].

There are two types of dyes used in DSSC, the first type is organometallic dyes such as Ruthenium complexes (N3 and N719) which is considered promising dye with a power conversion efficiency of around 13% under air mass (AM) 1.5 irradiation [9]. However, due to the high cost of noble metals such as Ru and Pd, pure organic dyes have been developed and used as an alternative active layer, so there are many examples of organic dye derivatives which give high efficiencies, such as triphenylamine, thienopyridine, fluorine, coumarin, and others [10-13]. Imidazole derivatives are one of the most promising organic compounds in DSSC due to their versatility and synthetic way, which has four substituted positions to give these derivatives more flexibility for designing with donor and acceptor part positions [14]. For instance, they behave as bipolar materials spatially if bonded with the donor part such as triphenylamine. The imidazole derivatives have good bipolar transport characteristics, wide absorption, and bright luminescence. The most important properties of imidazole are related to the auxiliary of donor electrons due to their conjugated chain. It has low charge recombination after electron injection into the TiO_2 nanoparticles, considering the decrease in the positive charge density on the donor surface by electron delocalization [15-17].

In general, the DSSC efficiency depends directly on HOMO and LUMO of the synthesizer as well as on the conduction band (CB) of the nano-metal oxide, therefore, the theoretical study with the deferent method has been proved to be the bright one to get the accurate energy levels for dyes in DSSC, so the computational studies give all information before prepared dyes which are saved time and money as well as gave reasonable results.

Based on the experimentally prepared dye C1, a novel four organic compounds are theoretically designed as a donor–spacer–acceptor group in this work [18]. All these designed compounds are studied by density functional theory (DFT) and time-dependent density functional theory (TD-DFT) to investigate the energy of HOMO and LUMO as well as geometries, energy gap, electronic distribution, and electronic absorption spectra.

Methods

Dye design

Four new virtual dyes as imidazole derivatives, were systemically designed according to the fixed experimentally prepared dye C1 for DSSCs (Figure 1). All dyes were designed by the same donor and acceptor parts but with different π-spacer and that is to investigate the rules of this conjugated spacer. The π-bridge was designed with two thiophene molecules, and two furan molecules, Thieno [3,2-b] thiophene and furo[3,2-b]furan for dyes C2, C3, C4, and C5, respectively. These spacers are chosen by donating atoms such as O or S to improve the conjugated system as well as improve the extended conjugation chain to decrease the energy gap and improve the color of the dye for more light absorption.

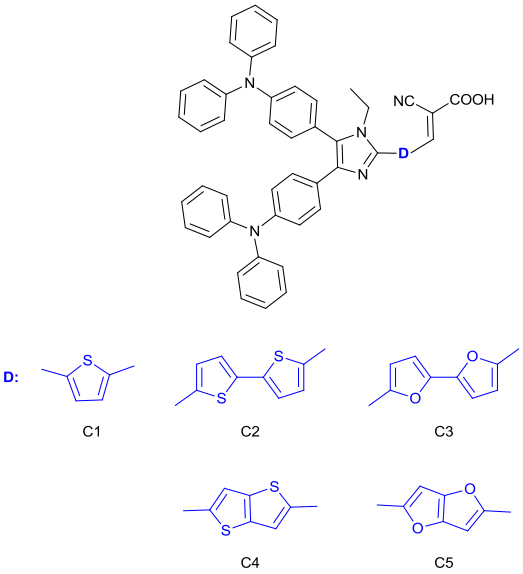

FIGURE 1 The experimentally prepared dye (C1) with four virtual dyes designed (C2, C3, C4, and C5)

Computational methods

All calculations were performed by using the program package (Gaussian 09W) [19,20]. The density functional theory (DFT) was performed for all dyes by using Becke's three-parameter hybrid function combined with the Lee-Yang–Parr correlation function (B3LYP) to simulate the structure and electronic transition levels [21]. The optimization frequency calculations were employed by base set B3LYP/6-311++G** to optimize structure geometry and calculate the energy level (HOMO-LUMO) for all dyes, as displayed in Figure 2. All the vibration frequencies were calculated with the same level of optimization geometry, and all vibration frequencies have no imaginary peaks, which indicates that the computational calculation of all dyes has true energy level minima. D-DFT with B3LYP/6-311++G** was used to calculate the oscillator strength (f) and absorption wavelength (max). All these optimized structures were obtained in a vacuum.

Results and discussions

Dye design and optimization

The criteria for choosing the dyes as an active layer are represented in many points; firstly, the structures of all molecules are prevented from the formation of the aggregate (π-stacked) efficiently due to the branch alkyl group which is bonded to nitrogen atoms in the imidazole part. Secondly, the electron distributions in all molecules have given a good separation between HOMO and LUMO and a good overlap on the π-bridge. Finally, all π-spacers were chosen to increase the conjugated system, which led to improving the light-harvesting of the dye [22,23].

The optimized geometries of the five dyes are displayed in Figure 2. The -bridge parts and accepters in all of these structures are coplanar, which provided a good continuous conjugated effect to transfer the excited electron from donor to TiO_2 surface, as well as the triphenylamine unit and alkyl group which bonded with imidazole, which helped to inhibit - sticking and improved dye solubility.

As depicted in Figure 2, all dye structures can be divided into five parts: the first part is the phenylamine group with the same side of arylamine (Pr) in the imidazole ring; the second part is the phenylamine with the same said of imine group (Pnr) in imidazole ring, the third part is the imidazole ring, the fourth one is the π-bridge part, and the last part is the cyanoacitc acid. According to this design, the electron distributions of the HOMOs for all dyes were mainly located in triphenylamine (Pnr) and imidazole units (Figure 3). The electron distributions of the LUMOs were essentially localized in π-spacer and cyano acetic acid parts, which indicates that there is a good charge separation between donor and acceptor in the molecules. Likewise, there is an overlap in electron distribution between HOMO and LUMO orbitals in the imidazole unit, which could lead to an intramolecular charge transfer from frontier molecular orbitals and it could be classified as a π-π* intramolecular charge transfer [24,25]. Moreover, the electron distribution of the LUMO was concentrated on the acceptor unit, which improved the overlap with the 3rd orbital in TiO_2 and gave a good electron injection between the molecule and the surface of TiO_2. Interestingly, the dipole moment of all the dyes was indicated some variation. For instance, the dipole moment of the thiophene molecular spacer was (C2 = 9.5, C4=9.7 Debyes) higher than the furan molecular spacer (C3=7.3, C5 = 7.9 Debyes).

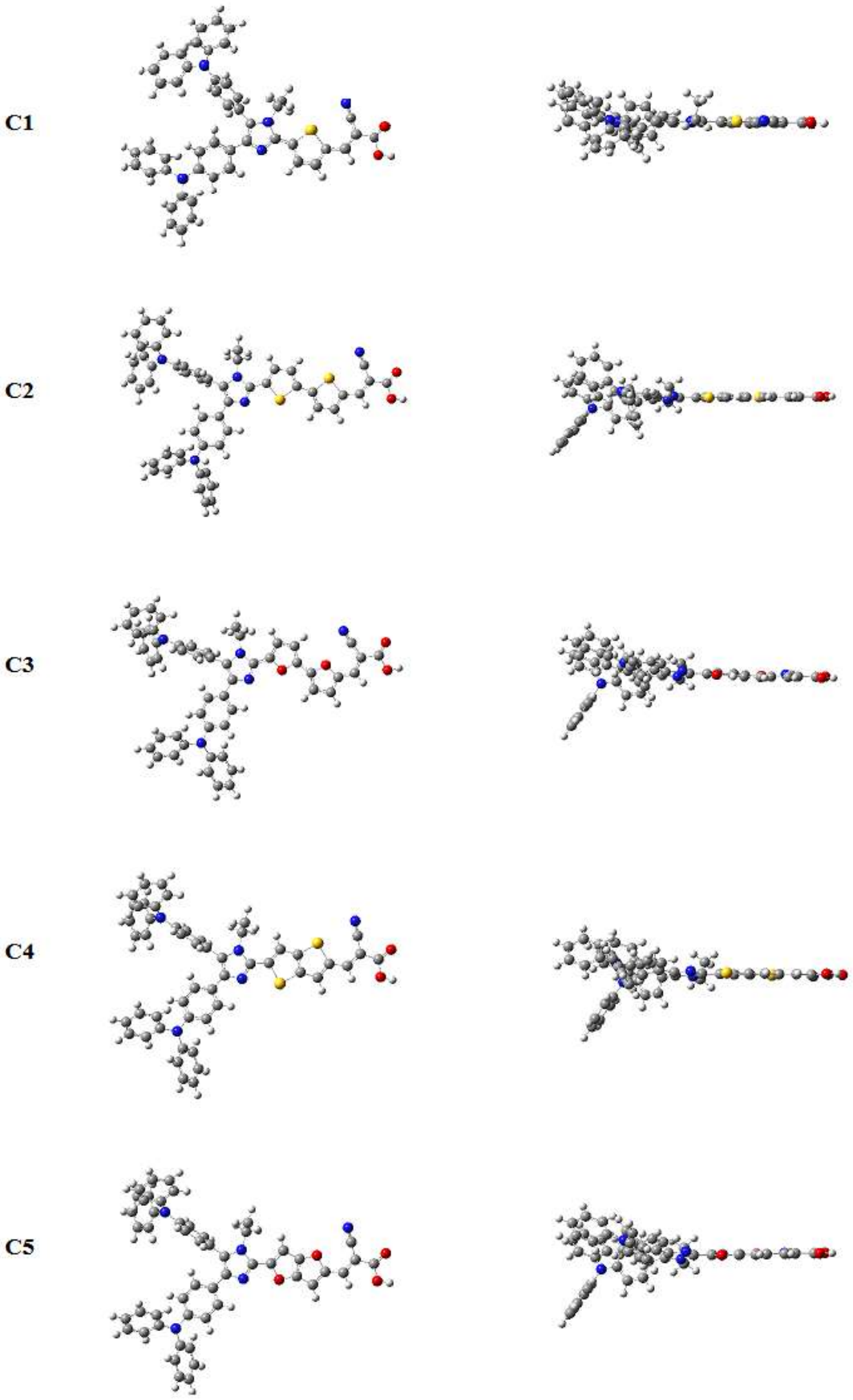

FIGURE 2 The optimized molecular structures of five dyes in a vacuum

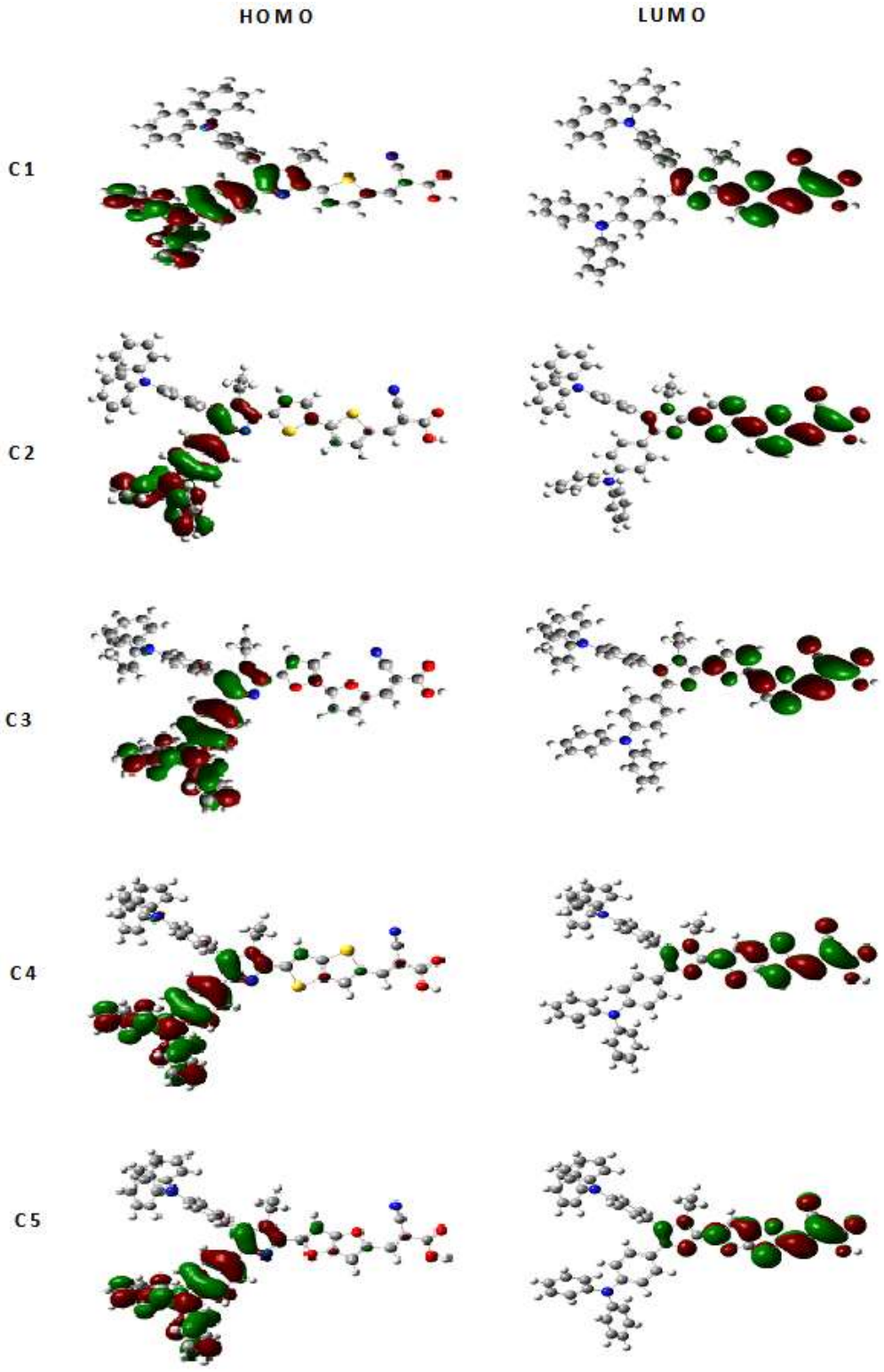

FIGURE 3 The electron distribution (HOMO and LUMO) for all dyes

Optical properties

The computational calculations of simulated absorption spectra for these dyes were calculated by the TD-DFT method and are displayed in Figure 4. All these dyes exhibited one broad absorption band except for C3 dye,

which had two broad absorption bands. The dye C3 (two furan spacers) had the highest absorption band λ_{max}=493 nm (Table 1), and the lowest absorption band at λ_{max}=363 nm was represented by dye C1 (two thiophene spacers). By comparing dyes, the C2 dye has a longer wavelength ~ 900 nm, which indicates that the harvest is more light than other ones. On the other hand, the C1 dye has a smaller wavelength~640 nm which impacts negatively on the power conversion efficiency of the solar cells. In Table 1, the λ_{max} of C1, C2, C3, C4, and C5 dyes represent the electron transitions of HOMO-0 → LUMO+0 (+68%), HOMO-0 → LUMO+0 (+69%), HOMO-0 → LUMO+0 (+70%), HOMO-0 → LUMO+0 (+68%) and HOMO-0 → LUMO+0 (+69%) respectively. In comparison with the original compound C1, all dyes have a redshift absorption peak with an energy gap of 2.03 eV for both C3 and C5, and an energy gap of 1.91 eV and 2.00 eV for dyes C2 and C4, respectively.

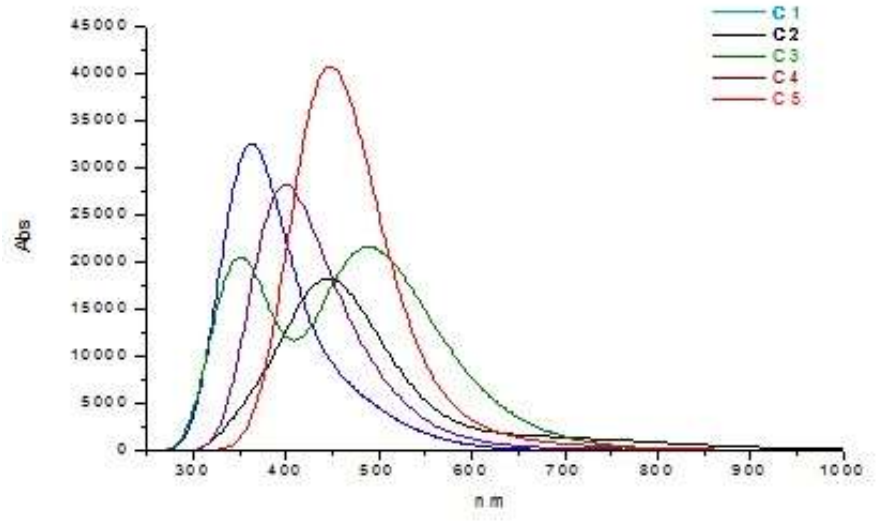

FIGURE 4 Simulated absorption spectra of C1, C2, C3, C4, and C5 dyes

All these compounds have two donor groups (Pr and Pnr) which have different effects on the molecule. The first donor group (Pr) was attached at position 5 on the imidazole part and allows the resonance with π-spacer and acceptor, while Pnr attached at position 4 on the imidazole part, which prevents a resonance. In general, the donor part (Pr) allows the resonance interaction between the donor and the rest of the molecule, which leads to small charge separation and higher oscillator strength, whereas the Pnr is expected to have a large charge separation and lower oscillator strength effect.

Table 1 indicates the energy gap, wavelength, and oscillator strength for all dyes and by comparison, the lowest energy gap (HOMO-0→LUMO+0) was represented by C2 dye (1.91 eV, two thiophene spacers), while the largest energy gap was represented by the original molecule C1 dye (2.08 eV, one thiophene spacer) as well as the lowest LUMO was represented by C2 dye (-3.12 eV) which led to a good electron injection from the LUMO to the conduction band (CB) of TiO_2 (Figure 5). On the other hand, all dyes have a good HOMO level with less than the energy level of the electrolyte solution of $I^-\backslash I_3^-$ (-4.80 eV), which illustrates that the electron is easy to back again to the donor parts by the injection driving force of the electrolyte solution, as well as the beast HOMO level represented by C3 dye (two furan molecules) and that is about -4.97 eV.

TABLE 1 The photovoltaic and optoelectronic properties of five dyes

Dyes	Egap(eV)	Wavelength (nm)	*E*(eV)	*f*	Composition
		686.04 nm	1.807	0.032	H-0→L+0,H-0→L+1
C1	2.08	481.00 nm	2.577	0.155	H-1→L+0,H-0→L+0
		462.97 nm	2.678	0.018	H-1→L+0,H-0→L+1
		487.00 nm	2.545	0.048	H-0→L+0
C2	1.91	447. 83 nm	2.768	0.090	H-1→L+1, H-1→L+2
		405.49 nm	3.057	0.007	H-0→L+1, H-0→L+2
		547.56 nm	2.264	0.134	H-0→L+0
C3	2.03	481.04 nm	2.577	0.441	H-1→L+0
		435.12 nm	2.849	0.018	H-2→L+0
		664.04 nm	1.867	0.003	H-0→L+0, H-0→L+1
C4	2.00	552.13 nm	2.249	0.008	H-1→L+0, H-1→L+2
		476.01 nm	2.604	0.060	H-0→L+0, H-0→L+1
		733.79 nm	1.689	0.001	H-0→L+0, H-0→L+1
C5	2.03	617.29 nm	2.008	0.018	H-1→L+0, H-1→L+2
		509.59 nm	2.433	0.039	H-0→L+0, H-0→L+1

The differences in π-bridge played a major role in the electron distribution, wavelength, and efficiency of the compound. In all spacers, the O and S were chosen by five-member ring conjugated molecules, which seemed to have a good stability against the oxidation or reduction process [26]. Replacement of the O atom increased the HOMO energy (figure 5) and can be found in compounds C3 (-4.97 eV) and C5 (-5.05 eV) when compared to C2 (-5.03 eV) and C4 (-5.07 eV), respectively, whereas the substitution of the S atom generally provided a larger area for electron delocalization between HOMO and LUMO. Furthermore, the substitution of the O atom tends to redshift the absorption peak, which is approximately 40 nm between C2 and C3 dyes and approximately 50 nm between C4 and C5, indicating that dyes with O substitution harvest more light than dyes with S substitution. On the other hand, the low energy gap or high light-harvesting did not indicate that the dye gave good efficiency because some other physical properties are affected directly by the efficiency, such as solubility and aggregation.

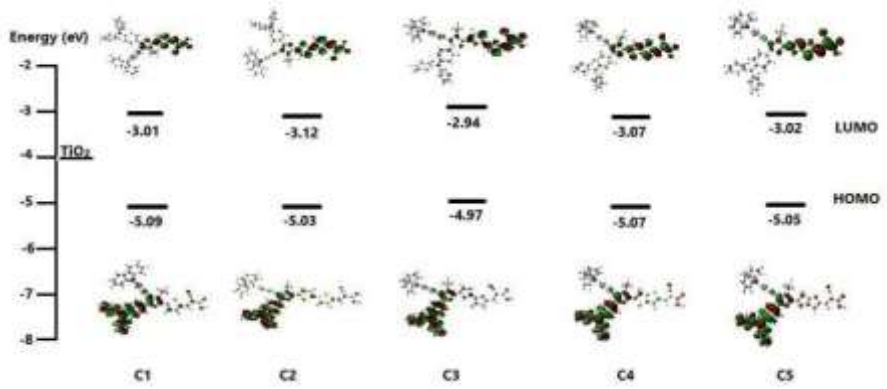

FIGURE 5 The electronic density distributions and the energy diagram of HOMO and LUMO of all dyes

Conclusion

In this work, the computational study of five donors, π-bridge, and acceptor dyes has been investigated by different spacer units which are designed to be used in DSSC devices. The ground state geometries and excited states have been investigated by DFT and TD-DFT methods, respectively. The optimization geometry of these dyes exhibits a good steric effect, which prevents the aggregation of molecules on the surface of TiO_2. In all dyes, the electrons of HOMO orbitals were delocalized in donor and imidazole parts, while the LUMO orbitals were delocalized into π-bridge and acceptor parts, which led to the good separation between orbitals and improved the efficiency of the dyes. Moreover, the LUMOs of these organic dyes are higher than the CB band of TiO_2 and the HOMOs are lower than that electrolyte solution I^-/I_3^- and because of these properties, all dyes designed are suitable for DSSCs. The modification of C2 dye by using two thiophene molecules as a spacer reduced the bandgap from 2.08 eV to 1.91 eV, which led to an improvement in the DSSC efficiency.

Acknowledgments

We gratefully acknowledge the Energy Department, College of Energy and Environmental Sciences, Al-Karkh University of Science and the Department of Chemistry, College of Science, the University of Kerbala for funding and support.

Orcid:

Saifaldeen Muwafag Abdalhadi:
https://orcid.org/0000-0003-4057-3893
Haitham Dalol Hanoon:
https://orcid.org/0000-0001-8108-4477

References

[1] J. Gong, K. Sumathy, Q. Qiao, Z. Zhou, *Renew. Sustain. Energy Rev.,* **2017**, *68*, 234-246. [Crossref], [Google Scholar], [Publisher]

[2] J. Ajayan, D. Nirmal, P. Mohankumar, M. Saravanan, M. Jagadesh, L. Arivazhagan, *Superlattices Microstruct.*, **2020**, *143*, 106549. [Crossref], [Google Scholar], [Publisher]

[3] N.S. Kumar, K.C.B. Naidu, *J. Materiomics.*, **2021**, *7*, 940-956. [Crossref], [Google Scholar], [Publisher]

[4] S.M. Abdalhadi, A.Y. Al-Baitai, H.A. Al-Zubaidi, *Indones. J. Chem.,* **2020**, *21*, 9. [Google Scholar], [Pdf]

[5] A. Mishra, M.K.R. Fischer, P. Bäuerle, *Angew. Chem. Int. Ed.*, **2009**, *48*, 2474-2499.[Crossref], [Google Scholar], [Publisher]

[6] S. Zhang, X. Yang, Y. Numata, L. Han, *Energy Environ. Sci.,* **2013**, *6*, 1443-1464. [Google Scholar], [Publisher]

[7] M. Cariello, S.M. Abdalhadi, P. Yadav, J.D. Decoppet, S.M. Zakeeruddin, M. Grätzel, A. Hagfeldt, G. Cooke, *Dalton Trans.*, **2018**, *47*, 6549-6556. [Crossref], [Google Scholar], [Publisher]

[8] K. Sharma, V. Sharma, S.S. Sharma, *Nanoscale Res Lett.,* **2018**, *13*, 381. [Crossref], [Google Scholar], [Publisher]

[9] S.M. Abdalhadi, A. Connell, X. Zhang, A.A. Wiles, M.L. Davies , P.J. Holliman, G. Cooke, *J. Mater. Chem.*, **2016**, *4*, 15655-15661. [Crossref], [Google Scholar], [Publisher]

[10] V. Sugathan, E. John, K. Sudhakar, *Renew. Sust. Energ. Rev.*, **2015**, *52*, 54-64. [Crossref], [Google Scholar], [Publisher]

[11] A. Jena, S.P. Mohanty, P. Kumar, J. Naduvath, V. Gondane, P. Lekha, J. Das, H.K. Narula, S. Mallick, P. Bhargava, *Trans. Indian Ceram. Soc.*, **2012**, *71*, 1-16. [Crossref], [Google Scholar], [Publisher]

[12] V.K. Singh, R.K. Kanaparthi, L. Giribabu, *Rsc Advances.*, **2014**, *4*, 6970-6984. [Crossref], [Google Scholar], [Publisher]

[13] C.P. Lee, R.Y.Y. Lin, L.Y. Lin, C.T. Li, T.C. Chu, S.S. Sun, J.T. Lin, K.C. Ho, *RSC Advances.*, **2015**, *5*, 23810-23825. [Crossref], [Google Scholar], [Publisher].

[14] X. Chen, C. Jia, Z. Wan, X. Yao, *Dyes Pigm.*, **2014**, *104*, 48-56.[Crossref], [Google Scholar], [Publisher]

[15] J. Tagare, D.K. Dubey, R.A.K. Yadav, J.H. Jou, S. Vaidyanathan, *Adv. Mater.,* **2020**, *1*, 666-679. [Crossref], [Google Scholar], [Publisher].
[16] S.M.J. Nabavi, H. Alinezhad, B. Hosseinzadeh, R. Ghahary, M. Tajbakhsh, *J. Electron. Mater.*, **2020**, *49*, 3735-3750. [Crossref], [Google Scholar], [Publisher]
[17] J. Sivanadanam, I.S. Aidhen, K. Ramanujam, *New J Chem.*, **2020**, *44*, 10207-10219. [Crossref], [Google Scholar], [Publisher]
[18] M. Velusamy, Y.C. Hsu, J.T. Lin, C.W. Chang, C.P. Hsu, *Chem Asian J.*, **2010**, *5*, 87-96. [Crossref], [Google Scholar], [Publisher]
[19] V.A. Rassolov, M.A. Ratner, J.A. Pople, P.C. Redfern, L.A. Curtiss, *J Comput Chem.*, **2001**, *22*, 976-984. [Crossref], [Google Scholar], [Publisher]
[20] V. Mohankumar, P. Pounraj, M. Senthil Pandian, P. Ramasamy, *Braz. J. Phys.*, **2019**, *49*, 103-112. [Crossref], [Google Scholar], [Publisher].
[21] A. Irfan, A.G. Al-Sehemi, *J. Saudi Chem. Soc.*, **2015**, *19*, 318-321.[Crossref], [Google Scholar], [Publisher]
[22] Y. Xie, W. Wu, H. Zhu, J. Liu, W. Zhang, H. Tian, W.H. Zhu, *Chem. Sci.*, **2016**, *7*, 544-549. [Crossref], [Google Scholar], [Publisher]
[23] W. Li, B. Liu, Y. Wu, S. Zhu, Q. Zhang, W. Zhu, *Dyes Pigm.*, **2013**, *99*, 176-184. [Crossref], [Google Scholar], [Publisher]
[24] A. Fitri, A.T. Benjelloun, M. Benzakour, M. McHarfi, M. Hamidi, M. Bouachrine, *Spectrochim. Acta A Mol. Biomol. Spectrosc.,* **2014**, *124*, 646-654. [Crossref], [Google Scholar], [Publisher].
[25] X. Chen, C. Jia, Z. Wan, J. Zhang, X. Yao, *Spectrochim. Acta A Mol. Biomol. Spectrosc.*, **2014**, *123*, 282-289. [Crossref], [Google Scholar], [Publisher]
[26] M.R. Detty, P.B. Merkel, *J Am Chem Soc.*, **1990**, *112*, 3845-3855. [Crossref], [Google Scholar], [Publisher]

How to cite this article: Saifaldeen Fahim Abdulhussein*, Saifaldeen Muwafag Abdalhadi, Haitham Dalol Hanoon. Investigation of the π-bridge role for imidazole derivative dyes in dye synthesized solar cell: theoretical study. *Eurasian Chemical Communications*, 2022, 4(7), 598-606. **Link:** http://www.echemcom.com/article_147347.html